University of California
Santa Barbara

Flow Regimes in a Rotating Multi-Cylinder Array

A Thesis submitted in partial satisfaction
of the requirements for the degree

Master of Science
in
Mechanical Engineering

by

Sean Kristopher Bohling

Committee in charge:

Professor Emilie Dressaire, Chair
Professor Elliot Hawkes
Professor Eckart Meiburg

June 2024

The Thesis of Sean Kristopher Bohling is approved.

Professor Elliot Hawkes

Professor Eckart Meiburg

Professor Emilie Dressaire, Committee Chair

June 2024

Flow Regimes in a Rotating Multi-Cylinder Array

by

Sean Kristopher Bohling

Acknowledgements

I would first like to thank Dr. Emilie Dressaire for her guidance and expertise without which this thesis would not exist. Thank you to all my lab mates, Dr. Sri Savya Tanikella, Sara Gonzalez, and Trinh Huynh, Jiayang Huang for all their support in the lab. Another instrumental figure with experimental advice was Dr. Brian Dincau. Finally, I would like to acknowledge my friends and family for their unwavering support throughout this work.

Abstract

Flow Regimes in a Rotating Multi-Cylinder Array

by

Sean Kristopher Bohling

Aquatic organisms extensively rely on hair-covered surfaces to perform functions ranging from chemical sensing to filter feeding. The flow over such hair-covered surfaces has traditionally been studied with a macroscopic array of rigid cylindrical hairs in a long flow channel. This channel geometry is a great starting point but does not necessarily provide a flow profile that matches the ones found in nature. Flow through such finite porous medium exhibits three regimes, with increasing fluid transport through the array: rake, deflection, and sieve. In the rake regime, the bulk flow is diverted around the array, while in the sieve regime, the flow goes through the array. The deflection regime is a transition regime where some of the streamlines exit the array laterally. The regimes depend on the Reynolds number of the flow, porosity, and confinement of the array. The channel geometry has previously been used as a model configuration to study transport. Here we introduce a new flow geometry where the array of hairs is swept in a circular path around a cylindrical tank, through stationary fluid. This flow condition has a velocity profile that linearly increases from the inner to outer edge of the array. To study the influence of the flow geometry on the three regimes, we vary the rotational velocity and array dimensions. Variables such as the flow rate entering the array through the first row and the drag on the hair array allow for the definition of the three regimes and the efficiency of the filtration process. These variables are first measured in Chapter 2 with 2D finite element analysis simulations using COMSOL Multiphysics. The filter efficiency increases with the volume of fluid entering the array and decreases with the

drag on the array. The filtered volume and drag coefficient exhibit a non-linear dependence on the rotation speed. In Chapter 3, we discuss the experimental methods used to obtain preliminary results that are able to quantify the transition from rake to deflection regimes for two arrays with different cylinder spacings. Our finding verify that the rake to deflection regime change can be experimentally found and measured.

Contents

Chapter 1

Introduction

Filter feeders are aquatic organisms that use intricate structures to sort food particles from water. Hair-like structures are commonly used to trap particles before they are ingested. The performance of those biological filters exceeds those of engineered systems. In particular, biological filters robustly capture food particles during the lifetime of the organisms [1, 2]. Engineered filters experience a decrease in efficiency as they get progressively clogged until they need to be replaced [3]. Filter feeders are found across various length scales, demonstrating the versatility of the approach. Therefore, biological hair-covered surfaces are a source of inspiration for improved water filtration systems, including industrial and domestic processes and more advanced applications, such as long-term space missions.

Porous media are commonly used to trap particles. Because of the small scale of the pores, the flow is characterized by a low to intermediate Reynolds number, $Re = \rho U \lambda / \mu$ where ρ and μ are the density and viscosity of the fluid respectively, U the average velocity of the flow and λ the size of the pores. Various filtration modes are involved in trapping suspended particles by solid surfaces: direct interception, inertial impaction, gravitational deposition, diffusion or motile-particle deposition, and electrostatic attraction [4]. Direct

interception is a common capture mode for non-Brownian, neutrally buoyant particles in a low Re flow [5].

To determine which particles are captured, it is necessary to model the flow through the porous medium or filter. For a finite array of fibers or cylinders, previous work has shown the existence of three distinct flow regimes in the Reynolds number range of 0.001-40 [6, 7, 8]. The regimes depend on the Reynolds number of the flow, porosity, and confinement of the array. The three regimes in order from lowest Re to highest Re are rake, deflection, and then sieve. In the rake regime, the flow does not enter the array but instead flows around it, creating a flow field similar to what is commonly observed around a bluff body. In the sieve regime, the fluid flows straight through the array, in the gaps between rows of cylinders, with a very low curvature in the streamlines. The deflection regime is intermediate: the flow enters the front of the array, and part of the fluid is diverted to the side, i.e., curved streamlines exit the array laterally.

This Thesis investigates the filtration capability of a bio-inspired hair array rotating in a cylindrical tank of quiescent fluid. The hair array comprises 25 cylinders of identical diameter arranged on a square lattice. We begin with a numerical study of the filtration process, presented in Chapter 2. The particle capture is assumed by direct interception for the low Reynolds number flows considered here. The multi-cylinder array is modeled as two-dimensional since the hairs used to filter in nature have large aspect ratios. The rotating array approximates the flow field experienced by aquatic creatures such as crustaceans, which flick their antennule in an arc [9]. Flow rate and drag measurements taken from finite element-based simulations allow us to identify the three flow regimes reported in previous studies and measure the filtration efficiency for a rotating array. Sections 2.1 and 2.2 of this thesis describe the numerical simulations and flow regimes. In section 2.3, we study the filtration capabilities of the array and analyze the power lost to drag. We conclude chapter 2 with a discussion of filtration efficiency and future

work. Chapter 3 discusses the experimental work that complements Chapter 2. There we start by describing the design of arrays and the fluid used in experiments. Next, we discuss the PIV methods used to extract experimental flow rates. Finally, we present the experimental flow rates used to recover the rake and deflection flow regimes.

Chapter 2

Numerical Simulations

2.1 Filtration Efficiency Simulations

2.1.1 Geometry and governing equations

The model two-dimensional filter is a 5x5 square array of cylinders that rotates along a circular trajectory in a circular domain, as shown in Figure 2.1. The circular domain is centered at point O and has a radius R_1. The domain is filled with a Newtonian fluid of density ρ and viscosity μ at rest. The array is composed of "infinite" cylinders that have a diameter d. The spacing between cylinders is noted δ, and measured from center to center. The array is at a distance R_2 from point O.

As the array moves through the fluid at rest, we rely on simulations to define the velocity and pressure field around the cylinders. We write mass and momentum conservation for Newtonian fluid and an incompressible flow. The Navier-Stokes and continuity equations read:

$$\rho \left[\frac{\partial \mathbf{u}}{\partial t} + (\mathbf{u} \cdot \nabla)\, \mathbf{u} \right] = \mu \nabla^2 \mathbf{u} - \nabla p \tag{2.1}$$

$$\nabla \cdot \mathbf{u} = 0 \tag{2.2}$$

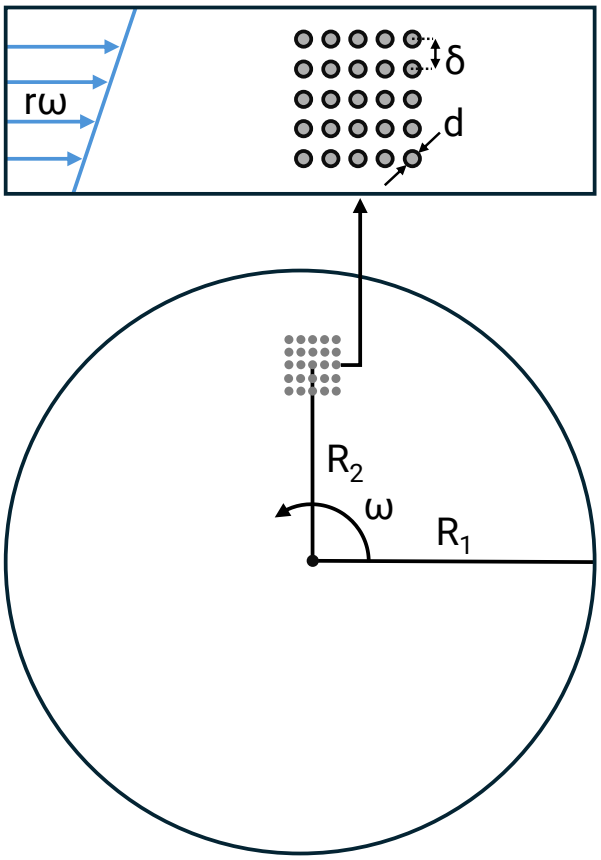

Figure 2.1: Schematic of cylinder array moving along a circular trajectory in a tank of fluid at rest.

We impose the following boundary conditions:

$$\mathbf{u} = 0 \quad \text{on cylinder walls} \tag{2.3}$$

$$\mathbf{u}(R_1) = 0 \quad \text{on tank walls} \tag{2.4}$$

2.1.2 Simulations

The governing equations are solved using a finite element method in COMSOL Multiphysics. The system is modeled in two dimensions, with the array rotating about the origin. The simulations use a moving mesh to move the array along a circular trajectory about O with an angular velocity $\omega = [6.67 \times 10^{-6} - 2.67 \times 10^{-1}]\ s^{-1}$. In all simulations, $R_1 = 30$ cm, $d = 1$ mm, $R_2 = 15$ cm, and $\delta = [2.5, 5]$ mm. The Reynolds number is defined using the hair diameter and the velocity at the center of the array.

$$Re = \frac{\rho d U_{mean}}{\mu} = \frac{\rho d R_2 \omega}{\mu} \tag{2.5}$$

The Reynolds number ranges from 10^{-3} to 40 with $\rho = 1000$ kg.m^{-3} and $\mu = 10^{-3}$ Pa.s. The mesh density adapts to the flow condition and, as such, is smallest on all boundaries. Free triangular meshing is used with a minimum mesh size of 1.2×10^{-2} mm and a maximum mesh size of 4 mm. All simulations are time-dependent, with a study time of 2000 seconds.

A single cylinder is used to verify the simulation results and compare different mesh sizes. Indeed, the drag coefficient for low Reynolds number flows around a single infinite cylinder in a uniform velocity field has been extensively studied. In this benchmark simulation, we define the drag coefficient of the 2D cylinder. The drag coefficient can be

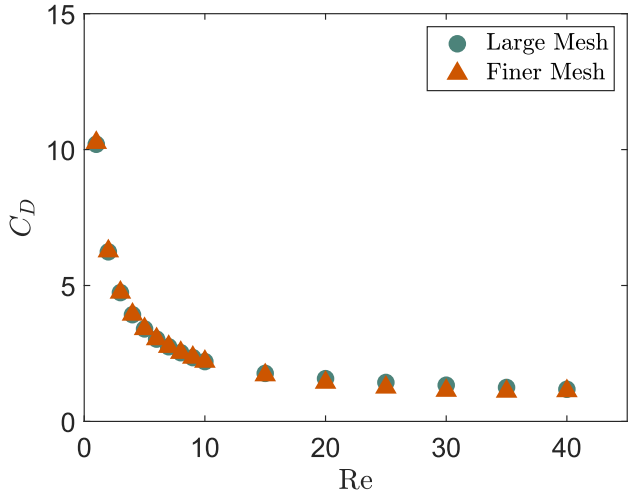

Figure 2.2: Drag coefficient of single cylinder

calculated with

$$C_D = \frac{\mathbf{F_D} \cdot \hat{\mathbf{x}}}{1/2\rho U_m^2 d} \tag{2.6}$$

where $\hat{\mathbf{x}}$ is a unit vector parallel to the flow and $\mathbf{F_D}$ is the total force on a cylinder which is defined as

$$\mathbf{F_D} = \int_{S_c} (p\mathbf{I} - \boldsymbol{\tau}) \cdot \hat{\mathbf{n}}\, dS_c \tag{2.7}$$

where S_c is the surface of the cylinder, p is the pressure, $\boldsymbol{\tau}$ is the shear stress tensor and $\hat{\mathbf{n}}$ is unit vector normal to the surface [10, 11, 12].

Figure 2.2 shows the measured drag coefficient for two mesh sizes. The finer and larger meshes are COMSOL user-defined physics-controlled meshes with a maximum mesh size of 2 and 4 mm, respectively. Since they produce identical results, all the simulations presented in this chapter use the larger mesh size to reduce computing time. The results also exhibit a Reynolds number dependence, similar to an infinite cylinder in a uniform flow [13, 12]. The comparison is not exact as our system has a finite domain, and the flow profile is not uniform, so we cannot compare the numerical values, yet the trends are identical. These results validate the simulation setup to study the flow through a 5x5

array of cylinders.

2.2 Flow Regimes

2.2.1 Bulk flow

Previous work has shown three flow regimes exist when fluid flows through an array of cylinders at Reynolds numbers of order 1 [7, 8]. These three regimes can be seen qualitatively by looking at the flow velocity for different Reynolds numbers. Figure 2.3 shows the fluid velocity for Reynolds numbers 0.1, 5, and 25, where the flow regimes transition from rake to deflection and finally to sieve. It is important to note that the fluid is at rest, and the array is moving. In the rake regime, the velocity of the fluid in the array is similar to the velocity of the cylinders. In the sieve regime, the fluid velocity between the cylinders is close to zero, as it is undisturbed by the moving cylinders. To compare our results with previous studies, we work in the moving frame of the reference of the array in what follows. We run simulations with a parameter sweep of the Reynolds numbers from 10^{-3} to 40, as the spacing of the cylinders is kept at a constant of $\delta = 5$ mm. At low flow rates, the array of cylinders acts as a rake, and most of the flow is diverted around the array, as seen in Figure 2.3(a). The array acts as a sieve at higher flow rates, and the flow goes through the array (Figure 2.3(c)). The deflection regime is the transition from rake to sieve where the flow enters the array but exits out the sides, as seen in Figure 2.3(b). Previous work has shown that the change of regimes can be related to the boundary layer thickness of a cylinder in the flow. At low Reynolds numbers, the boundary layers overlap and make the array act as a rake, while the high Reynolds number decreases the boundary layer thickness and allows the array to act as a sieve.

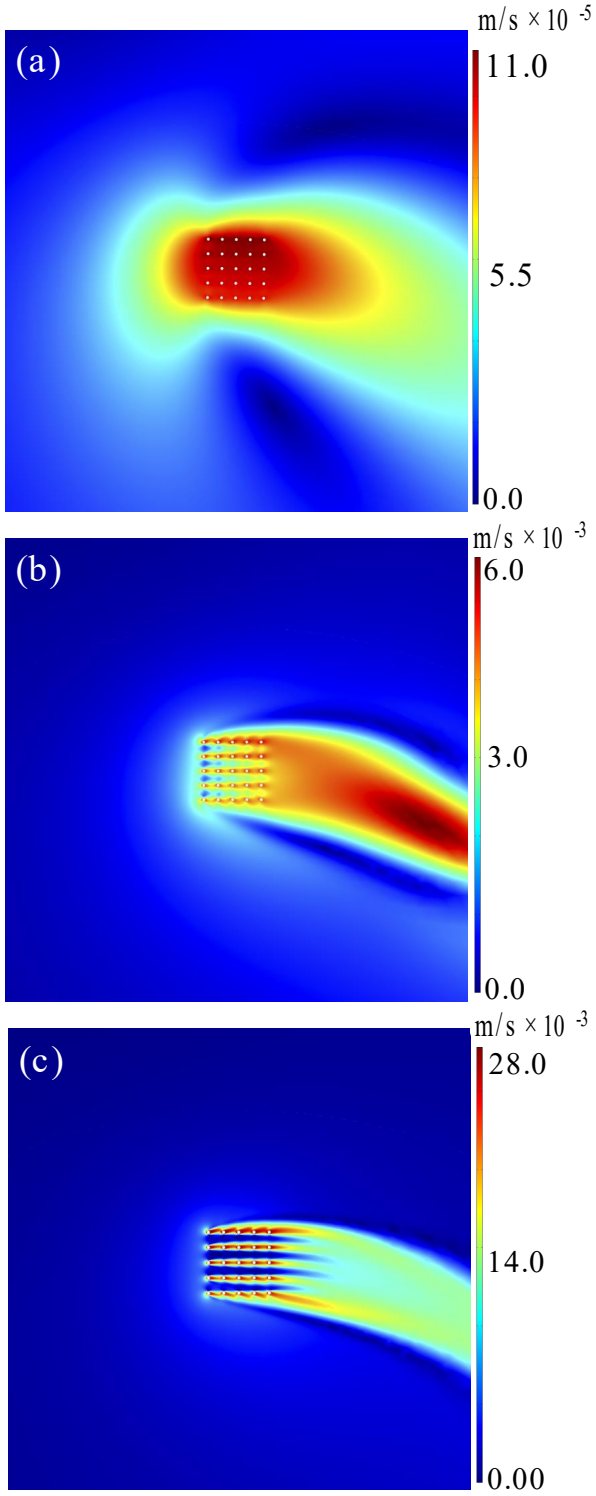

Figure 2.3: Flow fields for $\delta = 5$ mm at (a) $Re = 0.1$, in the rake regime (b) $Re = 5$, in the deflection regime (c) $Re = 25$, in the sieve regime

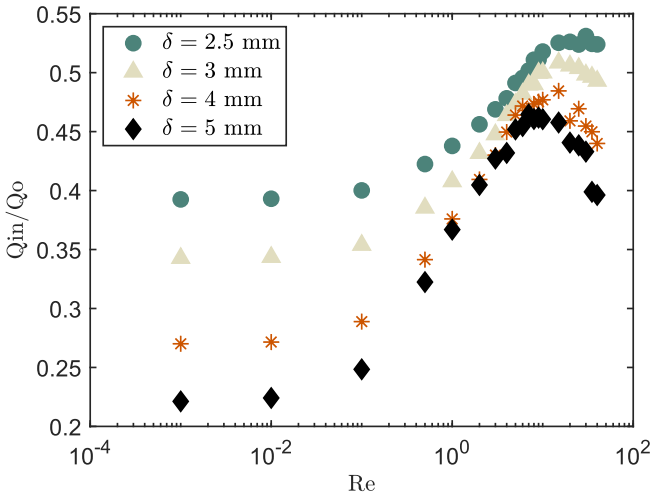

Figure 2.4: Evolution of Q_{in}/Q_o as a function of Re for multiple cylinder spacing.

2.2.2 Flow Rates

To further quantify the flow regimes, our study looks into the relationship between the flow rate entering the front of the array, Q_{in}, and the undisturbed flow rate, Q_0. Q_{in} was found by integrating the flow velocity over a line placed $0.5 \times \delta$ in front of the array and spanning from one edge to the other. This value was then divided by Q_0 to determine the percentage of bulk flow entering the array. The undisturbed flow Q_0 is the integral of the array velocity over the length of the leading edge:

$$Q_0 = \int_{R^-}^{R^+} \omega \, r dr \tag{2.8}$$

where $R^- = R_2 - 2\delta - d/2$ and $R^+ = R_2 + 2\delta + d/2$.

The results obtained for cylinder arrays with different spacings are shown in Figure 2.4 and exhibit three regimes. At low Re, in the rake regime, the ratio of flow rates is constant for each array spacing and has the lowest value since most of the flow goes around the array. As the array spacing increases, we see a decrease in the ratio of flow rates

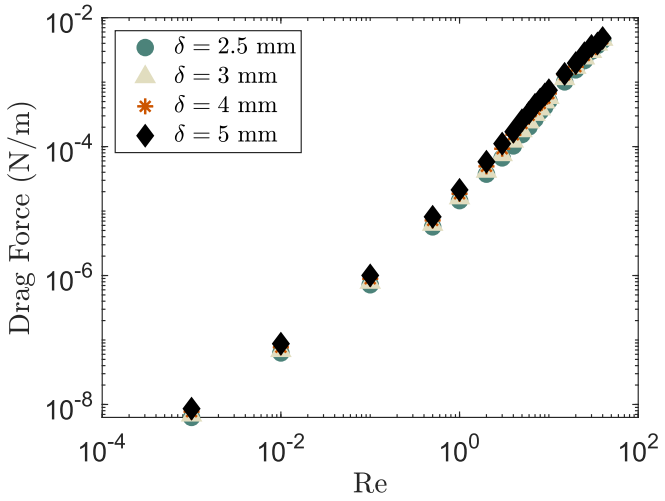

Figure 2.5: Drag force as a function of Re for multiple cylinder spacing.

because both Q_0 and Q_{in} grow with δ; however, Q_0 grows at a faster rate than Q_{in}. As a result, the largest fraction of flow entering the array is for the smallest spacing between cylinders. At a Reynolds number of approximately 0.1, the ratio becomes an increasing function of the Reynolds number. This growth continues until a Reynolds number of approximately 15, where the flow ratio levels off or begins to decrease depending on the array spacing. These two distinct regions correspond to the deflection and sieve regimes, respectively. The flow ratio increases with the deflection regime because the size of the boundary layer around each hair becomes smaller perpendicularly to the flow. The ratio reaches a maximum where Q_{in} can no longer grow faster than Q_0, leading to the plateau and decline in the ratio. We attribute this effect to the size and flow behavior of the recirculation region, which depends on their spacing.

2.2.3 Drag

We study the influence of the flow regimes on the drag force on the array. The drag force on the array is calculated using Equation 2.6 and summing the forces obtained

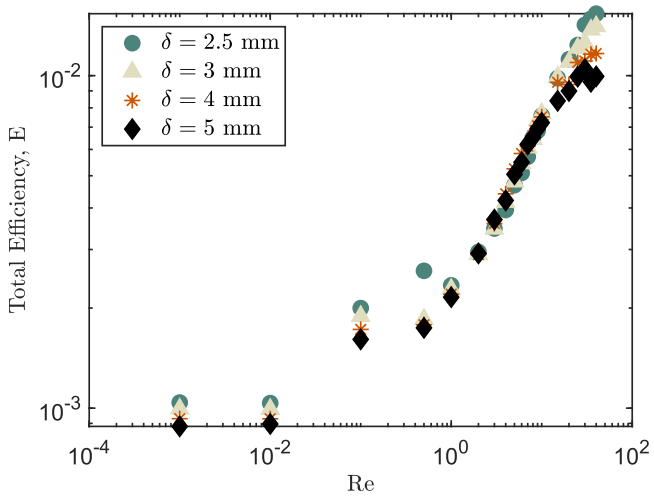

Figure 2.6: Total efficiency as a function of Re for multiple cylinder spacing.

for the 25 cylinders of the array. Figure 2.5 shows the drag force plotted against the Reynolds number for multiple spacing. No distinct regions are observed in the range of Reynolds numbers sampled: the drag force grows linearly with the Reynolds number. The flow regimes do not affect the drag force. The spacing of the cylinders impacts the total drag force. The drag force increases as the spacing increases. Since the drag force is known to vary with the area of the object, this dependence is consistent with our previous observation that the drag force does not depend on the flow regime.

2.3 Efficiency

We now consider how the flow regimes affect the filtration efficiency. Previous work indicates that particle capture results from direct interception at low Reynolds numbers. We assume that the filtered particles are smaller than the cylinder diameter and choose an arbitrary but representative diameter equal to $d_p = d/5$. The particles are captured if they travel along a streamline that comes near the cylinder [4]. For particles to come into contact with the cylinders, the distance between the streamline and the cylinder must be

smaller than or equal to the particle diameter. We, therefore, define an annular region around each cylinder, with an inner diameter of d and an outer diameter of $d + d_p$. To measure the amount of particles captured, we estimate the flow rate through the annular region in which the fluid is depleted of particles. The flow rate through the capture regions is called Q_c. We compare Q_c with the undisturbed flow Q_0 to determine how filter efficiency changes for different array spacing and Reynolds numbers.

We define the total efficiency of the array, $E = Q_c/Q_0$ as the fraction of undisturbed flow from which particles are removed. This definition allows to compare the array efficiency over a range of Reynolds numbers and for multiple array spacing, as seen in Figure 2.6. The efficiency shows a very similar trend to the relative flow rate entering the array Q_{in}/Q_0. The fluid fractions entering the array and filtered by the cylinders are constant for a low Reynolds number during the rake flow regime. The efficiency then increases with the Reynolds number through both the deflection and the sieve regimes. This result is consistent with direct interception being the only capture mechanism considered here. Indeed, as the relative amount of fluid entering the array increases, the amount of fluid flowing near the cylinders increases. At higher Re, inertial effects are expected to modify the capture probability and other mechanisms should be accounted for, such as inertial impact. We observe that a higher spacing leads to lower efficiency throughout all flow regimes. To rationalize these results, it is important to note that greater spacing means a large value of Q_0 because of the larger footprint of the array. This does not translate into an increased capture surface since the number of cylinders is set at 25.

Another metric to consider when designing a filter is the power consumption of the system. Our simulations allow to investigate the power loss due to drag on the array. This is accomplished by multiplying the drag force by the mean velocity, U_m. We can then compare the power needed to overcome the drag force to the amount of fluid filtered per unit time, Q_c. Figure 2.7 shows the power consumption per unit flow rate as a function of

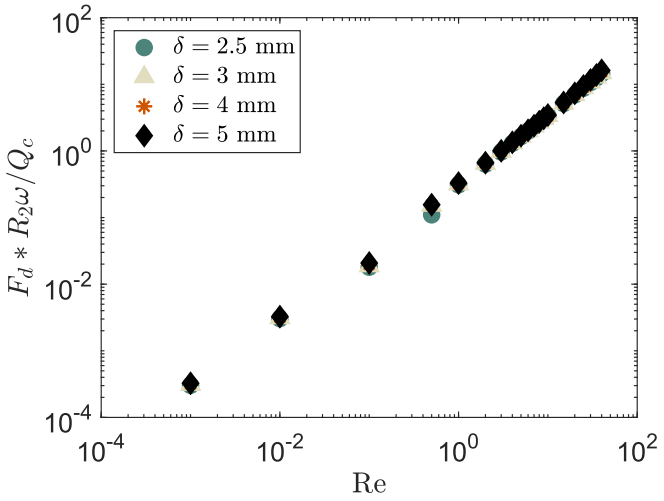

Figure 2.7: Power loss due to drag over Q_c as a function of Re for multiple cylinder spacing.

the Reynolds number. The monotonous increasing dependence of the power consumption on the Re or angular velocity of the array indicates that the filtration rate increases with the power required to overcome the drag. We note that the spacing between hairs does not dramatically affect Q_c and the drag on the array, which is consistent with the low permeability of the system. The result is valid for the range of Re considered. Indeed, at higher Re, one expects inertial effects to affect the capture efficiency, Q_c.

2.4 Conclusion

This study investigates the filtration capability of a rotating array of cylinders, assuming that particles are captured by direct interception at low Reynolds number flows. The study relies on numerical simulations in COMSOL Multiphysics. Flow rate measurements identify three distinct flow regimes that had only been reported in channel flows. These results are notable from (1) a fluid mechanics perspective, as the curvature of the streamlines does not affect the transport through the array, and (2) a practical viewpoint, as cylindrical tanks are commonly used for filtration processes. The efficiency

of the filtration process is quantified with the drag force on the array and the fraction of fluid from which particles are extracted. Both the efficiency and the power needed to overcome the drag are increasing functions of the Re number. The power consumption per unit flow rate increases with the Re in the low to intermediate Re range. Filtering fluid faster requires more power, but it also affects the mode of capture. A systematic study accounting for the different modes of capture and their capture probabilities would be necessary to describe the efficiency of the filter at higher Re numbers. Future work should also scale up the results presented here to filter larger fluid volumes.

Chapter 3

Multi-Cylinder Array Experiments

Expanding on the results of the numerical simulation study on filter efficiency, we designed and ran experiments to capture the properties of the flow through a multi-cylinder array of rigid cylinders. The goal of these experiments is to find a way to manufacture an array where the geometric parameters can be altered to modify the flow regimes through the array. Accomplishing this goal requires the design of such an array and the implementation of unique Particle Image Velocimetrty (PIV) techniques. The PIV techniques provide experimental flow rate results that can be utilized to determine the flow regime of the array. These experimental flow regimes can then be compared to the previously covered numerical simulation results. Once the experiments are verified, the array design will be extended to flexible hair-like cylinders which brings the research closer to the biological inspiration and closer to the design of large scale engineered bio-inspired filtration systems.

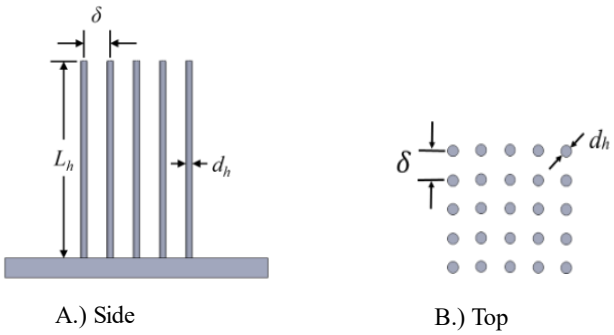

Figure 3.1: Dimensions of Multi-Cylinder array used in experiments

3.1 Array Design

3.1.1 Geometry and Materials

The bio-inspired model hair system used for the experimental portion of this thesis is a 5x5 square array of cylinders with a center to center spacing of δ, cylinder diameter d_h, and height of L_h. The main geometric parameter varied in experiments is the center to center spacing δ. These cylinders are made of fused silica and mounted into a laser cut acrylic sheet. For all experiments, L_h is 40 times larger than the diameter, D_h which allows for the experimentally measured flow rates to be compared to the two dimensional numerical simulations as the edge effects from the top of the cylinders and the base are minimum at the center.

3.1.2 Index Matching

The technique used for measuring flow velocities in this work is particle image velocimetry (PIV) which requires the use of a laser sheet to illuminate the flow. This means

that any shadows severely impact the measurements as particles are no longer be illuminated. Fused silica cylinders normally create shadows in water because of a mismatch in refractive index. Fused silica has a refractive index of 1.45 and water is 1.33. A common method or increasing the refractive index of water is to add glycerol. Since glycerol has a refractive index of 1.47 a mixture of water and glycerol can be made that matches the refractive index of fused silica and eliminates the shadow problem. The major downside to just mixing glycerol and water is the increase to the fluids viscosity. Glycerol has a viscosity of 1410 mPa·s which makes a solution of primarily glycerol difficult to work with experimentally. To reach a suitable refractive index without increasing the viscosity is to add urea to the water/glycerol mixture. Previous work has shown that a glycerol, water, and urea solution can be made to index match PDMS (RI=1.43) [14]. Building upon this study a 65/35 mixture of glycerol to water with 48 wt% in urea closely matched the index of refraction for fused silica and limited the effect of shadow in experimental measurements. The density of the solution used for all experiments is 1210 kg/m^3 and the viscosity is 17.1 mPa·s.

3.2 Particle Image Velocimetry

3.2.1 Experimental Setup

The experiments in this thesis use a Dantec PIV setup supported by Dantec Dynamics software. The experiment takes place in a large acrylic tank with diameter, R = 146 mm. The tank is filled with the index matched fluid,whose density and viscosity are ρ = 1210 kg/m^3 μ=17.1 mPa·s respectively. The fluid is stationary at the start of the experiment. The fluid is seed with 400 mg of 10 μm silver coated particles. The cylinder array is mounted on a rotating rod which rotates at a distance from the center, r = 50 mm. A

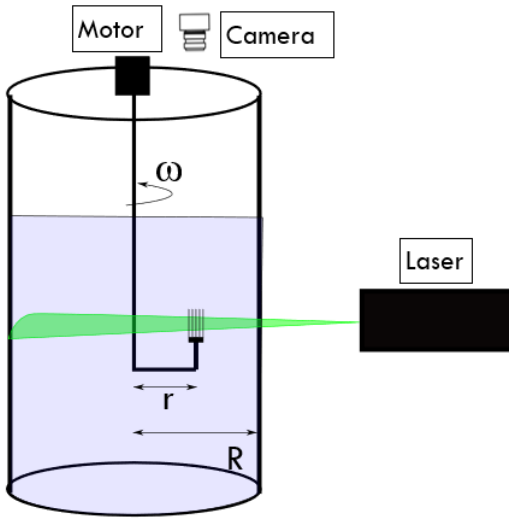

Figure 3.2: Schematic of experimental set up

camera is mounted above the tank and records the flow. A schematic of the experimental setup is shown in Figure 3.2. The experiments investigate flow through multi-cylinder arrays at Reynolds numbers ranging from 0.1 to 6 which corresponds to an angular velocity of 0.27 to 16.2 rpm. The experiments also investigates the array spacings, $\delta =$ [2 3]mm.

3.2.2 Methods

For each combination of δ and Reynolds number the array is allowed 10 minutes of rotation for the flow to develop. Once the flow has developed the camera records the array passing through the illuminated area 10-15 times. Each pass allows the camera to record 15-20 grey scale frames which are then stored and analysed in the PIV software.

The raw images from the camera cover a larger area than needed for the analysis so the images are cropped to better highlight the flow around the multi-cylinder array. The next step is to extract the location of the individual cylinders so that a mask can be generated. The tops of the cylinders are painted black to distinguish the array from the

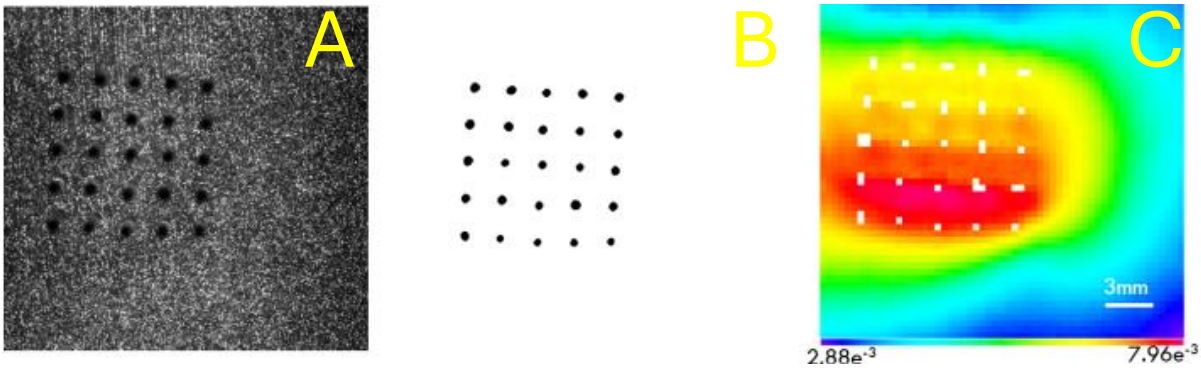

Figure 3.3: PIV method. A. Image recorded by camera, B. Mask identifying the position of the cylinders, and C. Velocity Field in the moving frame of reference

surrounding fluid and a pixel intensity threshold creates a moving mask that covers the array in each frame of the experiment. This moving mask can be seen in Figure 3.3B. Combining the moving mask with the cropped images allows for the use of the adaptive PIV function in the software which outputs a vector plot showing the particle velocities in each frame. The vector plot can be converted to a scalar map which shows the flow velocity and the moving mask as shown in Figure 3.3C. A line can then be drawn in front of the array on the scalar map to extract the velocities along that line for each frame. This data can then be analysed to determine a flow rate that is entering the array for all experiments. The flow rate is equivalent and can be compared to the Q_{in} described in the numerical simulation chapter of this thesis. The flow rate value measured in each frame is averaged to determine Q_{in} for that experimental parameter set

3.3 Preliminary results

To quantify the flow characteristics in theses experiments, we compare the flow rate entering the array, Q_{in} to the undisturbed flow rate,Q_o. This metric provides a measure

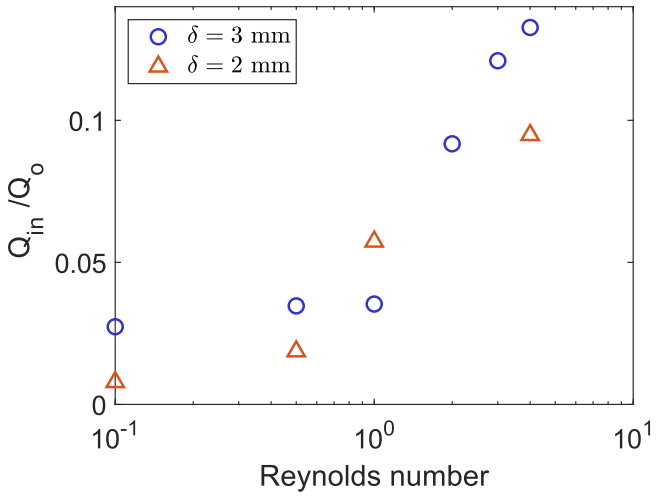

Figure 3.4: Experiment results of Q_{in}/Q_o for δ = 2,3 mm and multiple Re

of the percent of bulk flow entering the array. Q_{in} is found experimentally using the previously mention PIV methods and Q_o is found analytically. The undisturbed flow Q_0 is the integral of the array velocity over the length of the leading edge:

$$Q_0 = \int_{R^-}^{R^+} \omega \, r dr \tag{3.1}$$

where $R^- = r - 2\delta - d/2$ and $R^+ = r + 2\delta + d/2$.

The results for two cylinder arrays with different spacings are shown in Figure 3.4 and exhibit two of the three flow regimes shown in Chapter 2 with numerical simulations. At low Re the flow is in the rake regime and the ratio of flow rates is constant. At a Re of about 1 the ratio becomes an increasing function of Re. This is consistent with the numerical simulation results in Chapter 2. Experimental results do not extend past a Reynolds number of 6, therefore we have not yet recovered the third regime found with numerical simulations.

3.4 Conclusion

These experiments investigate the flow regimes present in a rotating array of cylinders utilizing particle image velocimetry. The experiments required the design and creation of two multi-cylinder arrays made of fused silica with different array spacings. The difference in refractive index between the cylinders and water requires the formulation of a low-viscosity solution that can index match fused silica without raising the viscosity higher than experimental viable. This solution was made with a combination of glycerol, water, and urea. During the PIV experiments, the flow rate into the array is measured for a variety of Reynolds numbers. Finally, we compare the flow rate evaluated to the undisturbed flow rate to quantify the transition from rake to deflection regimes.

Bibliography

[1] S. L. Sanderson, E. Roberts, J. Lineburg, and H. Brooks, *Fish mouths as engineering structures for vortical cross-step filtration*, *Nature Communications* **7** (2016), no. 1 11092.

[2] L. Hamann and A. Blanke, *Suspension feeders: diversity, principles of particle separation and biomimetic potential*, *Journal of the Royal Society Interface* **19** (2022), no. 186 20210741.

[3] E. Dressaire and A. Sauret, *Clogging of microfluidic systems*, *Soft Matter* **13** (2016), no. 1 37–48.

[4] D. I. Rubenstein and M. A. R. Koehl, *The Mechanisms of Filter Feeding: Some Theoretical Considerations*, *The American Naturalist* **111** (1977), no. 981 981–994.

[5] V. Rastegar, G. Ahmadi, and S. V. Babu, *Effect of flow velocity on fiber efficiency and particle residence time during filtration of aqueous dispersions—An experimental and simulation study*, *Particulate Science and Technology* **37** (2019), no. 2 161–170.

[6] A. Y. L. Cheer and M. A. R. Koehl, *Paddles and rakes: Fluid flow through bristled appendages of small organisms*, *Journal of Theoretical Biology* (1987).

[7] K. Hood, M. S. S. Jammalamadaka, and A. E. Hosoi, *Marine crustaceans with hairy appendages: Role of hydrodynamic boundary layers in sensing and feeding*, *Physical Review Fluids* **4** (2019), no. 11 114102.

[8] S. S. Tanikella, N. D. Jones, and E. Dressaire, *A Numerical Study of the Effect of Surface Coverage on the Filtration Performance of Hair Arrays*, vol. Volume 10: Fluids Engineering of *ASME International Mechanical Engineering Congress and Exposition*, p. V010T10A031, 11, 2021.

[9] M. A. R. Koehl, J. R. Koseff, J. P. Crimaldi, M. G. McCay, T. Cooper, M. B. Wiley, and P. A. Moore, *Lobster Sniffing: Antennule Design and Hydrodynamic Filtering of Information in an Odor Plume*, *Science* **294** (2001), no. 5548 1948–1951.

[10] A. Nicolle and I. Eames, *Numerical study of flow through and around a circular array of cylinders*, *Journal of Fluid Mechanics* **679** (2011) 1–31.

[11] T. Tang, P. Yu, X. Shan, J. Li, and S. Yu, *On the transition behavior of laminar flow through and around a multi-cylinder array*, *Physics of Fluids* **32** (2020), no. 1 013601.

[12] A. Khalili and B. Liu, *Stokes' paradox: creeping flow past a two-dimensional cylinder in an infinite domain*, *Journal of Fluid Mechanics* **817** (2017) 374–387.

[13] T. Tang, P. Yu, X. Shan, H. Chen, and J. Su, *Investigation of drag properties for flow through and around square arrays of cylinders at low Reynolds numbers*, *Chemical Engineering Science* **199** (2019) 285–301.

[14] M. C. Brindise, M. M. Busse, and P. P. Vlachos, *Density- and viscosity-matched Newtonian and non-Newtonian blood-analog solutions with PDMS refractive index*, *Experiments in Fluids* **59** (2018), no. 11 173.